Electrochemical Surface Oxidation Enhanced Raman Scattering

*Juan V. Perales-Rondon[a], Sheila Hernandez[a], Daniel Martin-Yerga[b], Pablo Fanjul-Bolado[b], Aranzazu Heras[a], Alvaro Colina[a]**

[a]Department of Chemistry, Universidad de Burgos, Pza. Misael Bañuelos s/n, E-09001 Burgos, Spain.

[b]DropSens, Edificio CEEI, Parque Tecnológico de Asturias, 33428 Llanera, Asturias, Spain.

Abstract

In this work, an unexpected enhancement of the Raman signal for uric acid during the electrochemical oxidation of a silver electrode is presented. This behavior cannot be easily explained using classical models of Surface Enhanced Raman Scattering (SERS). Time resolved Raman spectroelectrochemistry is used to study this interesting process strongly dependent on the experimental conditions. The new phenomenon was observed in different molecules and was found to be reproducible and robust, allowing us to use this methodology for the determination of citric acid. The enhancement of the Raman signal only takes place when a potential is applied to the electrode and therefore, this new phenomenon can be denoted as Electrochemical Surface Oxidation Enhanced Raman Scattering (EC-SOERS). In this work, EC-SOERS is presented not only as an

alternative to SERS for detection of molecules but also as a reproducible process that can be used for quantitative analysis.

Keywords: SERS; silver roughening; Raman spectroelectrochemistry; PARAFAC.

1. Introduction

Silver roughened electrode [1] is one of the most used substrates in Surface Enhanced Raman Scattering (SERS), due to its plasmonic properties [2,3] and the ease of preparation. The roughening process is widely known in literature and implies the surface oxidation (Ag dissolution) and the subsequent Ag^+ reduction on the electrode. During this process, formation of Ag nanoparticles (NPs) [4–6], responsible for the SERS electromagnetic effect, takes place. This deposition yields a much higher area and a nanostructured roughened surface, which modifies its optical properties, and ultimately, modulate the SERS behavior [7]. A number of works propose different ways to generate roughened silver substrates, from using cyclic voltammetry (CV) to applying a step potential program [8,9]. Most of the cases include the presence of chloride (Cl^-) or other halide, which allows getting higher silver dissolution and promoting the nanostructuration after the reduction stage [8,9]. Despite this process has been widely characterized in literature [10,11], its dynamic evolution in presence of a Raman probe molecule has been scarcely studied.

SERS has been widely used for analysis, not only by using Raman spectroscopic signal but also by combining this one with electrochemistry to quantify different analytes at a controlled potential [12,13]. In the present work, time-resolved

Raman spectroelectrochemistry [14–17] (TR-Raman SEC) is used to follow the roughening process of silver with a Raman probe molecule in the electrolytic solution, being possible to detect transient processes [18–20]. Thus, SERS SEC system allows both, the electrochemical investigation and also the simultaneous SERS data, and therefore presents wide applicability in target molecules analysis with low detection limit. Interestingly, when using uric acid (UA) as a probe molecule, it was found a special and unexpected enhancement of the Raman signal at the electrochemical oxidation stage of a silver substrate. Thus, an equivalent process to SERS is observed, that can be denoted as Surface Oxidation Enhanced Raman Scattering (SOERS). Unlike classical SERS, this effect was only observed during the electrochemical oxidation of the silver electrode surface. Therefore, it should be denoted as Electrochemical-SOERS (EC-SOERS). This effect was potential dependent and exclusively observed for particular experimental conditions. To the best of our knowledge, this is the first time that such behavior is reported in the literature. This result, in principle, does not match any classical SERS result reported in bibliography, which suggests the loss of the Raman signal during silver oxidation [21–23].

In order to illustrate the usefulness of EC-SOERS for analysis, citric acid was selected as target analyte. This compound is used extensively in the manufacturing of carbonated beverages, fruit and vegetable drinks, cheeses and other dairy products. It is also a natural component of many fruits and vegetables, and also an important component of certain corporal fluids. [24–26]. One of the main advantages of using TR-Raman SEC as analytical technique is the intrinsic trilinear character of the responses obtained by SEC that can be used for multi-way data [27]. Thus, using PARAFAC as a chemometric tool, Raman SEC data

could provide information about both the concentration of a test sample and the evolution of the spectra during a voltammetric experiment.

This work is a first approach to this interesting enhancement of the Raman signal during the oxidation of the silver electrode that, as is demonstrated, can be used for analytical purposes.

2. Experimental

2.1. Reagents and Materials

Perchloric acid ($HClO_4$, 60 %, reagent, Sigma-Aldrich), uric acid (UA, 99+%, reagent, ACROS Organics), potassium chloride (KCl, 99+%, reagent, ACROS Organics), pyridine (Py, 99.5%, analysis, Merck), benzoic acid (BzA, 99.5%, PA, Panreac) and potassium cyanide (KCN, 99%, PRS, Panreac) were used. All solutions were prepared using ultrapure water obtained from a Millipore DirectQ purification system provided by Millipore (18.2 MΩ cm resistivity at 25 °C).

2.2. Instrumentation

Raman spectroelectrochemistry. In situ time-resolved Raman spectroelectrochemistry (TR-Raman-SEC) was performed by using a SPELEC RAMAN instrument (DropSens), which integrates a laser source of 785 nm. Laser Power in all experiments was 80 mW (254 $W \cdot cm^{-2}$). This instrument was connected to a bifurcated reflection probe (DRP-RAMANPROBE, Dropsens). Two Raman spectroelectrochemical cells were employed: a commercial cell for screen-printed electrodes (DRP-RAMANCELL, Dropsens) [12], and a home-made cell to carry out those experiments using a customized silver disk electrode. DropView SPELEC software (Dropsens) was used to control the instrument, which allows getting real-time and synchronized spectroelectrochemical data.

A home-made customized silver disk electrode was used as a working electrode. This consisted in a silver disk inserted in Teflon. In this experimental set-up, a home-made Ag/AgCl electrode and a platinum wire were used as reference and counter electrodes, respectively. Screen-printed silver electrodes (DRP-C013, DropSens) were also used for some experiments. These devices consist of a flat ceramic card on which a three-electrode system comprising the electrochemical cell is screen-printed. The working silver electrode is circular with a diameter of 1.6 mm, the auxiliary electrode is made of carbon and a silver paint acts as a pseudoreference.

UV-vis spectroscopy. UV-vis absorption experiments were carried out using an UV-vis spectrophotometer Cary 50 Conc (Viarian). Solutions were sampled using a standard quartz cuvette 10 x10 mm.

SEM microscopy. A JEOL 6610LV scanning electron microscope (SEM) was used to characterize the working silver electrodes at various stages of the electrochemical activation. Images were recorded with the secondary electron detector and using an accelerated voltage of 20 kV.

Electrochemical impedance spectroscopy (EIS). An Autolab PGSTAT 302N potentiostat equipped with a FRA module of impedance was used to carry out the EIS experiments. Differential capacitances were obtained by measuring the real (Z') and imaginary (Z") components of the impedance at 20 constant frequencies ranging from 0.1 Hz to 1000 Hz, with the potential being stepped in a sequence of 0.025 V and 0.05 V, from +0.10 V to -0.55 V vs Ag/AgCl.

3. Results and discussion

3.1. Electrochemical Surface Oxidation Enhanced Raman Scattering (EC-SOERS)

In an attempt to obtain suitable information about the appearance of an EC-SOERS signal during the electrochemical oxidation of a silver substrate, UA Raman response was evaluated in acidic media, using TR-Raman SEC. To achieve this, a linear sweep voltammetry (LSV) along a proper potential window was applied, recording simultaneously the Raman response with a high time-resolution. Fig. 1 presents the Raman spectra for UA 0.2 mM recorded during a LSV experiment and the evolution of the Raman intensity at 641 cm^{-1} as a function of the applied potential for two different electrolytic media ($HClO_4$ 0.1 M and $HClO_4$ 0.1 M + KCl $5 \cdot 10^{-3}$ M), scanning the potential from +0.1 V to +0.55 V. For simplicity in the terminology, this plot will be called voltaRamangram because it represents the evolution of the Raman intensity at a specific Raman shift as a function of the applied potential in a voltammetric experiment.

As can be observed in Fig. 1a, when the LSV is carried out in $HClO_4$ 0.1 M ($HClO_4$), there is no appreciable peaks in the Raman spectrum corresponding to UA in the whole potential window, fact corroborated in the voltaRamangram at 641 cm^{-1} for UA in this media (blue curve in Fig. 1d). However, when some small amount of Cl^- is added ($5 \cdot 10^{-3}$ M), unexpectedly, significant unusual Raman signal were observed (Fig. 1b) corresponding unmistakably to uric acid spectrum [28,29].

Fig. 1

Fig. 1b shows the Raman spectra for UA 0.2 mM + $HClO_4$ 0.1 M + KCl $5 \cdot 10^{-3}$ M ($HClO_4$/KCl) recorded at different potentials during the LSV (Table S1 shows the band

assignment, and Fig. S1 shows a comparison of UA Raman spectra under different experimental conditions). Interestingly, the enhancement of the Raman signal appeared at the oxidation stage of the silver roughening process (red curve in Fig. 1d), which does not match any previous SERS results during a spectroelectrochemical experiment. A closer look at Fig. 1d shows an increment of the Raman intensity above +0.20 V in the anodic direction, reaching a maximum around +0.50 V. Finally, red curve in Fig. 1c reveals that the increment of Raman signal is closely related with the LSV which support that oxidation products should be responsible for such singular effect.

More interesting results were obtained by recording the Raman spectra during a chronoamperometry (CA). Fig. 2 displays two SEC experiments at fixed potentials, collecting both Raman spectra and transient current responses simultaneously. In a first experiment, the potential was kept at +0.40 V for 60 s. In a second experiment, a potential of +0.40 V was applied for 30 s, time at which the electrode was left at open circuit potential (OCP) and the Raman spectra were recorded for other 30 s (Fig. 2b).

Fig. 2

The Raman intensity for UA at 641 cm^{-1} as a function of time (chronoRamangram) for the two experiments is represented in Fig. 2. As can be observed, the application of +0.40 V provoked the increase of the Raman intensity during the whole experiment. These CA experiments corroborate the responses observed in Fig. 1d, the anodic polarization (oxidation) of the electrode yields the increment of the UA Raman signal in these electrolytic conditions, in contrast to the typical SERS response that usually is observed at cathodic potentials [9,28–30]. It is noteworthy that Raman signal is lost at OCP (Fig. 2b), indicating that the phenomenon is potential dependent.

Different experiments using commercial silver screen printed electrodes (Ag-SPEs) were also made, demonstrating that voltammetric features were fairly similar with those obtained for a silver disk electrode (Fig. S2). Additionally, comparable results were obtained in two independent laboratories, which demonstrate the robustness and reproducibility of the phenomenon (Fig. S3).

It is noteworthy that the Raman signal is concentration dependent. A calibration curve was carried out using Ag-SPEs. Fig. S4a displays the voltaRamangrams at 641 cm^{-1} for different UA concentrations. The voltammetry features are fairly similar to that corresponding to a silver electrode, as was stated before in Fig. S2. Fig. S4b shows the fitting between the Raman intensity at 641 cm^{-1} and the UA concentration. A good linear relationship (R^2=0.99) was obtained, which means that the phenomenon is not due to a particular UA concentration. Furthermore, EC-SOERS is very reproducible and could be used for quantitative analysis.

3.2. Microscopic characterization of the Silver disk roughened electrode

To shed more light into the reason for this unusual SERS signal, SEM images were taken at different steps of the LSV (Fig. 3), using the same electrolytic media ($HClO_4$/KCl) and a silver disk electrode. At the early oxidation stage (Fig. 3a), it could be distinguished the incipient formation of AgCl particles [31,32], which evolve in shape and size at more positive potential values to generate bigger cubic AgCl particles (Fig. 3b). EDX analysis confirmed the composition of the cubic particles (Fig. S5 and Table S2) and revealed a silver enrichment of the AgCl cubic particles [33,34] along the anodic process, where the Raman signal enhancement is observed. Additionally, the voltammetric profile (Fig. S6) is in agreement with the SEM images and some earlier studies about the electrochemistry of silver electrodes [35,36] in different electrolytic

media. It is well known that AgCl does not present SERS effect, however an increment of Raman response for pyridine and other molecules adsorbed on Ag^+/AgCl or Ag/AgCl complex have been reported [37–40]. Finally, it is worth noting that, despite SEM images help to explain the observed enhancement, the Raman increment is lost when the electrode is left at OCP (Fig. 2). Therefore, only SEM results are not sufficient to fully understand the phenomenon.

Fig. 3

3.3. Explanation for EC-SOERS phenomenon

Rationalizing these results in terms of a SERS-like behavior, there are some possible reasons for the observed phenomenon. The first one is the formation of some silver nanoparticles as a result of the incident laser. The use of visible lasers to produce silver nanoparticles due to a photoreduction of Ag^+ is well documented [41,42]. In order to demonstrate whether such effect is the responsible for the observed phenomenon, similar experiments using typical Raman probe molecules were performed. Fig. 4 shows the voltaRamangrams and the CVs for pyridine (Py), potassium cyanide (KCN), benzoic acid (BzA) and UA in the same experimental conditions than those used for UA ($HClO_4$/KCl).

Fig. 4

In order to have a proper comparison between the four mentioned molecules, the SEC study was conducted along a complete CV to reproduce a silver oxidation-reduction cycle (ORC). In this sense, according to the classical SERS effect model, Py and CN^- Raman signals (Fig. 4a and 4b) increased just after the second silver reduction (for more details about the CVs see Fig. S6). However, at the oxidation stage, there was no

appreciable Raman signal for these two probe molecules. On the contrary, the increment of SERS signal for BzA (Fig. 4c) and UA (Fig. 4d) exclusively appeared during the oxidation stage, even in the cathodic direction. In fact, the corresponding voltaRamangrams show the same shape along the whole potential window. Moreover, when the experiment was started with the laser switched off, a Raman response was obtained at anodic potentials when the laser was switched on (data not shown). Additionally, experiments at different laser powers were performed in order to discard a possible photoreduction by the incident laser. Fig. S7a shows the evolution of the SOERS signal for UA at 641 cm^{-1} at the anodic vertex potential with the laser power. As expected, there is a decrease of the SOERS signal with the laser power, falling drastically from 0.29 to 0.13 mW. However, if SOERS signal is compared with the Raman signal obtained from a silicon test sample by applying the same laser power, a linear relationship between the two signals is observed (Fig. S7b). This relationship demonstrates that changes of SOERS intensity are only due to the laser power, and no other process such as photoreduction is taking place under these experimental conditions. Therefore, it can be concluded that the laser itself is not the responsible for such Raman signal enhancement.

In the case of UA, SEM images and EDX analysis were also obtained at different potentials during the cathodic scan (Fig. S5 and Table S2). The images confirm the presence of cubic AgCl particles and EDX values corroborate the silver enrichment of these particles which is expected at these potentials because of the Ag^+ reduction.

Another explanation could be related with the possibility of having a chemical and/or electrochemical reaction produced by the presence of Ag^+ species. However, if an oxidation and/or electrochemical reaction was occurring, the spectrum in the oxidation stage should be different from that recorded over cathodic potentials, that is to say, a

shifting of the Raman peaks in the spectra related to UA should be observed during the voltammetric experiment [28,29]. Fig. S8a shows a regular Raman spectrum during the experiment, which discards any change in the molecule during the whole ORC. Moreover, UA bands do not show any shifting with potential, as can be observed Fig. S8b.

A third possible explanation could be a SERS signal as a result of a Raman resonance effect. Nevertheless, this should be discarded due to the lack of formation of any Ag(I)-UA complex absorbing in the visible region. The latter has been demonstrated by collecting the UV-vis absorption spectra for a mixture of UA and $AgClO_4$ (Fig. S9a). Moreover, EC-SOERS behavior can be observed using different laser wavelengths (Fig. S9b). UA spectra can be observed during silver oxidation in experiments performed with three different lasers, 532 nm, 638 nm and 785 nm. Therefore, EC-SOERS is not wavelength dependent.

One more possibility could be the appearance of the SERS signal due to an electrochemical adsorption of UA or BzA at these potentials. It is well known that some compounds could adsorb on the electrode surface without any charge transfer [43–45]. For silver, the potential of zero charge (PZC) takes values closer to -0.70 V vs SCE [46,47], which implies that at potentials above +0.20 V is favored the adsorption of species that present affinity for silver surfaces. The pzc value is influenced by the electrolytic media and the presence of adsorbed species [48,49]. EIS experiments in our electrolytic solution (Fig. S10) could help to shed more light into the adsorption behavior of the species on the silver disk electrode. Fig. S10a and S10b represent the Z'-Z" curves at two potentials for the solution containing Cl^-, while Fig. S10c displays the differential capacitance for a silver electrode in $HClO_4$ 0.1 M + KCl $5 \cdot 10^{-3}$ M + UA 0.2 mM and in $HClO_4$ 0.1 M + UA 0.2 mM. The analysis of the data (Fig. S10c) reveals

that the presence of species with a specific surface adsorption (such as Cl^- or UA) could increase the differential capacitance as a consequence of the specific adsorption on the electrode surface. On the other hand, as has been demonstrated in previous works, the presence of an adsorbing species makes impossible to measure the pzc under these conditions [48]. EIS analysis indicates that an adsorption process is taking place in our electrolytic solution. Thus, at potentials above +0.20 V, the surface coverage of the analyte could be increased as a result of an electrochemical adsorption. Since SERS phenomenon depends on the distance between the substrate and the molecule, it would be reasonable to think that, the more favored the molecular adsorption, the bigger should be the SERS response observed, provided that a SERS substrate is involved in the process. That is to say, two key processes are required to register a SERS increment at these potentials: 1) the electrochemical adsorption or electrostatic closeness of the molecule to the surface, and 2) the existence of a proper SERS substrate that promote the enhancement itself either, by an electromagnetic mechanism or by a chemical enhancement.

In order to demonstrate whether the phenomenon is caused, mainly, by an electrochemical adsorption effect on a typical SERS substrate, an experiment using CN^- as a probe molecule was performed (Fig. 4b). The evaluation of Fig. 4b reveals that SERS effect is exclusively observed in the reduction stage [50,51]**.** Therefore, despite this molecule is negatively charged and present high affinity for a silver substrate (which should promote its adsorption), the electrochemical adsorption itself does not promote the appearance of any SERS signal at anodic potentials. This suggests that, although the electrochemical adsorption could be playing an important role in the appearance of a SERS signal, is not the main responsible for the observation of a Raman enhancement for UA or BzA.

Additionally, as was aforementioned, an increment of the Raman signal for some molecules adsorbed on Ag^+/AgCl or Ag/AgCl complexes have been reported [37–39]. Thus, the interaction of the target molecule with this complex could be another reason for such enhancement observed in the case of UA or BzA. This interaction could be deduced from the voltaRamangram at 243 cm^{-1}, where the Ag-Cl vibration takes place (Fig. S11a) [52,53]. As can be observed in Fig. S11b, when silver is oxidized, the intensity of Ag-Cl band increases up to +0.40 V. From this potential onwards, the Raman intensity for this band decreases concomitantly with the growth of the UA band. In the backward scan, the opposite process is observed. The Ag-Cl band increases when the UA band decreases, demonstrating a clear interaction between Ag^+/AgCl or Ag/AgCl particles and UA molecules.

3.4. Quantitative determination using EC-SOERS

Once described this interesting phenomenon, in this section, EC-SOERS was used for quantitative analysis. As a proof of concept, we have selected the determination of citric acid to show that different molecules can be detected using EC-SOERS. As was stated above, spectroelectrochemistry is an intrinsic trilinear technique. Therefore, PARAFAC [27,54] is a very suitable chemometric tool not only to assess the concentrations of unknown samples but also to understand the evolution of the signals related to the individual components of the sample. Actually, the determination of citric acid can be performed at a fixed Raman shift as is demonstrated in Fig. S12. However PARAFAC helps to deconvolve the Raman spectra and the evolution of the Raman signal with potential, which allows separating the contribution of the different components present in the spectroscopic response [27,54].

A calibration curve was performed using 6 citric acid concentrations in the range from 25 µM to 250 µM. Two different test samples (0.125 mM and 0.223 mM) were measured for studying the capability of prediction of the method. Cyclic voltammetry was selected to carry out the calibration experiments by scanning the potential starting at 0.00 V in the anodic direction (CV vertex potentials: -0.40 V and +0.40 V) at 0.02 $V \cdot s^{-1}$. A constrained PARAFAC model assuming the non-negativity of the concentrations was applied. Fig. S13 shows the deconvolution of the signals (concentration, spectra and its evolution with potential) of the samples. The main advantage of the PARAFAC model is that the scores of the citric acid concentrations are easily resolved because of the trilinearity of the data (orange points in Fig. 5). Two components can be resolved by the PARAFAC model. These components are citric acid (orange curve in Fig. S13b and S13c) and perchlorate (blue curve in Fig. S13b and S13c), that shows a typical Raman band at 950 cm^{-1} and 937 cm^{-1} respectively.

As can be observed, the evolution of the concentrations/spectra profiles with the potential, resolved by the PARAFAC model, shows the enhancement of citric acid during the oxidation processes along the voltammetric cycle, orange curve in Fig. S13c, demonstrating the EC-SOERS behavior. More interestingly, the evolution of the concentration/spectra profiles with potential for the perchlorate anion, blue curve in Fig. S13c, indicate that a small enhancement of its Raman scattering is obtained not only during the reduction of the AgCl nanoparticles (below 0.00 V) but also during the beginning of the oxidation (around +0.20 V) which could explain the silver enrichment of the AgCl NPs observed by EDX.

Fig. 5

Using the calibration curves the concentration of two problem samples with concentration 0.125 mM and 0.223 mM of citric acid were predicted (green points in Fig. 5) by performing a linear regression with the scores of the first PARAFAC component with the concentration of the calibration samples. The corresponding values of 0.127 mM and 0.233 mM (recoveries of 101.8 % and 104.6 %, respectively) for the two test samples demonstrate that EC-SOERS can be accurately used for quantitative analysis.

4. Conclusions

From the results discussed above it can be inferred that the chemical structure of the target molecule and its interaction with the substrate are dramatically important for the EC-SOERS signal observed during the anodic process. Taking into account that the AgCl nanostructures are enriched in silver at this stage, and the Raman enhancement at the oxidation process has been only observed in presence of Cl^-, the most probable explanation lies in the formation of a nanostructure that yields a SERS behavior, just after the first silver oxidation. Since Raman enhancement is discarded in presence of Ag^+ ion, the formation of Ag^+/AgCl or Ag/AgCl surfaces [37,55,56] could be the nanostructure responsible for such observed phenomenon, whose formation is mainly favored at anodic potentials. Furthermore, this effect, together with the electrochemical induced surface coverage could create the perfect environment to promote the enhancement of the Raman signal at these potentials. However, more powerful *in-situ* techniques that provide complementary information should be used to support this last hypothesis, in order to unravel this unexpected enhancement of the Raman signal during the silver electrochemical oxidation. Finally, as was demonstrated before, EC-SOERS is a very interesting alternative to classic SERS for determination of some particular

analytes, and should be studied in a deeper way to expand the application of the present phenomenon.

5. Acknowledgments

Authors acknowledge the financial support from Ministerio de Economía y Competitividad (Grants CTQ2017-83935-R, CTQ2014-55583-R, and CTQ2015-71955-REDT) and Junta de Castilla y León (Grant BU033-U16). J.V.P-R. thanks JCyL for his postdoctoral fellowship (Grant BU033-U16). S.H. thanks its contract funded by JCyL, the European Social Fund and the Youth Employment Initiative.

6. Supplementary material

Supplementary material contains the following supplementary material: CVs for the silver ORC, Raman spectra for UA, additional EC-SOERS experiments. SEM images and EDX analysis. UV-vis experiments for UA and $AgClO_4$ solutions. PARAFAC analysis and plots for loadings and scores from PARAFAC.

7. References

[1] M. Fleischmann, P.J. Hendra, A.J. McQuillan, Raman spectra of pyridine adsorbed at a silver electrode, Chem. Phys. Lett. 26 (1974) 163–166. doi:10.1016/0009-2614(74)85388-1.

[2] S.-Y. Ding, E.-M. You, Z.-Q. Tian, M. Moskovits, Electromagnetic theories of surface-enhanced Raman spectroscopy, Chem. Soc. Rev. 46 (2017) 4042–4076. doi:10.1039/C7CS00238F.

[3] A.B. Zrimsek, N. Chiang, M. Mattei, S. Zaleski, M.O. McAnally, C.T. Chapman, A.-I. Henry, G.C. Schatz, R.P. Van Duyne, Single-Molecule Chemistry with Surface- and Tip-Enhanced Raman Spectroscopy, Chem. Rev. 117 (2017) 7583–7613. doi:10.1021/acs.chemrev.6b00552.

[4] F.-R.F. Fan, A.J. Bard, Chemical, Electrochemical, Gravimetric, and Microscopic Studies on Antimicrobial Silver Films, J. Phys. Chem. B. 106 (2002) 279–287. doi:10.1021/jp012548d.

[5] M.L. Rodríguez-Sánchez, M.J. Rodríguez, M.C. Blanco, J. Rivas, M.A. López-

Quintela, Kinetics and Mechanism of the Formation of Ag Nanoparticles by Electrochemical Techniques: A Plasmon and Cluster Time-Resolved Spectroscopic Study, J. Phys. Chem. B. 109 (2005) 1183–1191. doi:10.1021/jp046056n.

[6] D. Buceta, N. Busto, G. Barone, J.M. Leal, F. Domínguez, L.J. Giovanetti, F.G. Requejo, B. García, M.A. López-Quintela, Ag 2 and Ag 3 Clusters: Synthesis, Characterization, and Interaction with DNA, Angew. Chemie Int. Ed. 54 (2015) 7612–7616. doi:10.1002/anie.201502917.

[7] M.D. Sonntag, J.M. Klingsporn, A.B. Zrimsek, B. Sharma, L.K. Ruvuna, R.P. Van Duyne, Molecular plasmonics for nanoscale spectroscopy, Chem. Soc. Rev. 43 (2014) 1230–1247. doi:10.1039/C3CS60187K.

[8] Z.-Q. Tian, B. Ren, D.-Y. Wu, Surface-Enhanced Raman Scattering: From Noble to Transition Metals and from Rough Surfaces to Ordered Nanostructures, J. Phys. Chem. B. 106 (2002) 9463–9483. doi:10.1021/jp0257449.

[9] X.-M.M. Lin, Y. Cui, Y.-H.H. Xu, B. Ren, Z.-Q.Q. Tian, Surface-enhanced Raman spectroscopy: substrate-related issues., Anal. Bioanal. Chem. 394 (2009) 1729–45. doi:10.1007/s00216-009-2761-5.

[10] Y.-C. Liu, C.-C. Yu, S.-F. Sheu, Low concentration rhodamine 6G observed by surface-enhanced Raman scattering on optimally electrochemically roughened silver substrates, J. Mater. Chem. 16 (2006) 3546. doi:10.1039/b609417a.

[11] C. Xiao, X. Chu, Y. Yang, X. Li, X. Zhang, J. Chen, Hollow nitrogen-doped carbon microspheres pyrolyzed from self-polymerized dopamine and its application in simultaneous electrochemical determination of uric acid, ascorbic acid and dopamine., Biosens. Bioelectron. 26 (2011) 2934–9. doi:10.1016/j.bios.2010.11.041.

[12] D. Martín-Yerga, A. Pérez-Junquera, M.B. González-García, J. V. Perales-Rondon, A. Heras, A. Colina, D. Hernández-Santos, P. Fanjul-Bolado, Quantitative Raman spectroelectrochemistry using silver screen-printed electrodes, Electrochim. Acta. 264 (2018) 183–190. doi:10.1016/j.electacta.2018.01.060.

[13] A.M. Robinson, S.G. Harroun, J. Bergman, C.L. Brosseau, Portable Electrochemical Surface-Enhanced Raman Spectroscopy System for Routine Spectroelectrochemical Analysis, Anal. Chem. 84 (2012) 1760–1764. doi:10.1021/ac2030078.

[14] B. Ren, Y. Cui, D.-Y. Wu, Z.-Q. Tian, Electrochemical SERS and its Application in Analytical, Biophysical and Life Science, in: Surf. Enhanc. Raman Spectrosc., Wiley-VCH Verlag GmbH & Co. KGaA, Weinheim, Germany, 2010: pp. 191–218. doi:10.1002/9783527632756.ch9.

[15] Y. Zhai, Z. Zhu, S. Zhou, C. Zhu, S. Dong, Recent advances in spectroelectrochemistry, Nanoscale. 10 (2018) 3089–3111. doi:10.1039/C7NR07803J.

[16] C. Shi, W. Zhang, R.L. Birke, D.K. Gosser, J.R. Lombardi, Time-resolved SERS, cyclic voltammetry, and digital simulation of the electroreduction of p-nitrobenzoic acid, J. Phys. Chem. 95 (1991) 6276–6285. doi:10.1021/j100169a040.

[17] D. Ibañez, E.C. Romero, A. Heras, A. Colina, Dynamic Raman spectroelectrochemistry of single walled carbon nanotubes modified electrodes using a Langmuir-Schaefer method, Electrochim. Acta. 129 (2014) 171–176. doi:10.1016/j.electacta.2014.02.094.

[18] D. Ibañez, C. Fernandez-Blanco, A. Heras, A. Colina, Time-Resolved Study of the Surface-Enhanced Raman Scattering Effect of Silver Nanoparticles Generated in Voltammetry Experiments., J. Phys. Chem. C. 118 (2014) 23426–23433. doi:10.1021/jp5074363.

[19] D. Ibañez, J. Garoz-Ruiz, A. Heras, A. Colina, Simultaneous UV–Visible Absorption and Raman Spectroelectrochemistry, Anal. Chem. 88 (2016) 8210–8217. doi:10.1021/acs.analchem.6b02008.

[20] C. Zong, C.-J. Chen, M. Zhang, D.-Y. Wu, B. Ren, Transient Electrochemical Surface-Enhanced Raman Spectroscopy: A Millisecond Time-Resolved Study of an Electrochemical Redox Process, J. Am. Chem. Soc. 137 (2015) 11768–11774. doi:10.1021/jacs.5b07197.

[21] D.-Y. Wu, J.-F. Li, B. Ren, Z.-Q. Tian, Electrochemical surface-enhanced Raman spectroscopy of nanostructures, Chem. Soc. Rev. 37 (2008) 1025. doi:10.1039/b707872m.

[22] T. Shegai, A. Vaskevich, I. Rubinstein, G. Haran, Raman spectroelectrochemistry of molecules within individual electromagnetic hot spots, J. Am. Chem. Soc. 131 (2009) 14392–14398. doi:10.1021/ja904480r.

[23] L. Zhao, J. Blackburn, C.L. Brosseau, Quantitative Detection of Uric Acid by Electrochemical-Surface Enhanced Raman Spectroscopy Using a Multilayered Au/Ag Substrate, Anal. Chem. 87 (2015) 441–447. doi:10.1021/ac503967s.

[24] G. Tyagi, D.K. Jangir, P. Singh, R. Mehrotra, R. Ganesan, E.S.R. Gopal, Rapid determination of main constituents of packed juices by reverse phase-high performance liquid chromatography: an insight in to commercial fruit drinks, J. Food Sci. Technol. 51 (2014) 476–484. doi:10.1007/s13197-011-0502-1.

[25] M. Castellari, A. Versari, U. Spinabelli, S. Galassi, A. Amati, An improved HPLC method for the analysis of organic acids, carbohydrates, and alcohols in grape musts and wines, J. Liq. Chromatogr. Relat. Technol. 23 (2000) 2047–2056. doi:10.1081/JLC-100100472.

[26] G. Zeppa, L. Conterno, V. Gerbi, Determination of Organic Acids, Sugars, Diacetyl, and Acetoin in Cheese by High-Performance Liquid Chromatography, J. Agric. Food Chem. 49 (2001) 2722–2726. doi:10.1021/jf0009403.

[27] N. González-Diéguez, A. Colina, J. López-Palacios, A. Heras, Spectroelectrochemistry at screen-printed electrodes: Determination of

dopamine, Anal. Chem. 84 (2012) 9146–9153. doi:10.1021/ac3018444.

[28] C. Westley, Y. Xu, B. Thilaganathan, A.J. Carnell, N.J. Turner, R. Goodacre, Absolute Quantification of Uric Acid in Human Urine Using Surface Enhanced Raman Scattering with the Standard Addition Method, Anal. Chem. 89 (2017) 2472–2477. doi:10.1021/acs.analchem.6b04588.

[29] L. Zhao, J. Blackburn, C.L. Brosseau, Quantitative Detection of Uric Acid by Electrochemical-Surface Enhanced Raman Spectroscopy Using a Multilayered Au/Ag Substrate, Anal. Chem. 87 (2015) 441–447. doi:10.1021/ac503967s.

[30] D.D. Tuschel, J.E. Pemberton, J.E. Cook, SERS and SEM of roughened silver electrode surfaces formed by controlled oxidation-reduction in aqueous chloride media, Langmuir. 2 (1986) 380–388. doi:10.1021/la00070a002.

[31] V.I. Birss, C.K. Smith, The anodic behavior of silver in chloride solutions—I. The formation and reduction of thin silver chloride films, Electrochim. Acta. 32 (1987) 259–268. doi:10.1016/0013-4686(87)85033-8.

[32] X. Jin, J. Lu, P. Liu, H. Tong, The electrochemical formation and reduction of a thick AgCl deposition layer on a silver substrate, J. Electroanal. Chem. 542 (2003) 85–96. doi:10.1016/S0022-0728(02)01474-2.

[33] B. Bozzini, G. Giovannelli, C. Mele, Electrochemical dynamics and structure of the Ag/AgCl interface in chloride-containing aqueous solutions, Surf. Coatings Technol. 201 (2007) 4619–4627. doi:10.1016/j.surfcoat.2006.09.127.

[34] H. Ha, J. Payer, The effect of silver chloride formation on the kinetics of silver dissolution in chloride solution, Electrochim. Acta. 56 (2011) 2781–2791. doi:10.1016/j.electacta.2010.12.050.

[35] S. Bharathi, K.L.N. Phani, G.P. Rao, Electrochemical behaviour of polycrystalline silver in solutions containing tetraphenylborate anion, J. Electroanal. Chem. Interfacial Electrochem. 289 (1990) 291–296. doi:10.1016/0022-0728(90)87224-8.

[36] B.M. Jović, V.D. Jović, D.M. Dražić, Kinetics of chloride ion adsorption and the mechanism of AgCl layer formation on the (111), (100) and (110) faces of silver, J. Electroanal. Chem. 399 (1995) 197–206. doi:10.1016/0022-0728(95)04291-1.

[37] Y.-F. Cheng, Q. Cao, J. Zhang, T. Wu, R. Che, Efficient photodegradation of dye pollutants using a novel plasmonic AgCl microrods array and photo-optimized surface-enhanced Raman scattering, Appl. Catal. B Environ. 217 (2017) 37–47. doi:10.1016/j.apcatb.2017.05.021.

[38] L. Dawei, W. Jian, X. Houwen, S. Xu, L. Fan-chen, Enhancement origin of SERS from pyridine adsorbed on AgCl colloids, Spectrochim. Acta Part A Mol. Spectrosc. 43 (1987) 379–382. doi:10.1016/0584-8539(87)80120-4.

[39] N. Zhao, X. Fei, X. Cheng, J. Yang, Synthesis of silver/silver chloride/graphene oxide composite and its surface-enhanced Raman scattering activity and self-cleaning property, in: IOP Conf. Ser. Mater. Sci. Eng., IOP Publishing, 2017: p.

12002. doi:10.1088/1757-899X/242/1/012002.

[40] Z. Gan, A. Zhao, M. Zhang, D. Wang, W. Tao, H. Guo, D. Li, M. Li, Q. Gao, A facile strategy for obtaining fresh Ag as SERS active substrates, J. Colloid Interface Sci. 366 (2012) 23–27. doi:10.1016/J.JCIS.2011.09.052.

[41] M. V. Cañamares, J. V. Garcia-Ramos, J.D. Gómez-Varga, C. Domingo, S. Sanchez-Cortes, Ag Nanoparticles Prepared by Laser Photoreduction as Substrates for in Situ Surface-Enhanced Raman Scattering Analysis of Dyes, Langmuir. 23 (2007) 5210–5215. doi:10.1021/la063445v.

[42] Y. Kang, H. Zhang, L. Zhang, T. Wu, L. Sun, D. Jiang, Y. Du, *In situ* preparation of Ag nanoparticles by laser photoreduction as SERS substrate for determination of Hg^{2+}, J. Raman Spectrosc. 48 (2017) 399–404. doi:10.1002/jrs.5044.

[43] G. Horányi, E.M. Rizmayer, J. Kónya, Radiotracer study of anion adsorption at silver electrodes in acidic medium, J. Electroanal. Chem. Interfacial Electrochem. 176 (1984) 339–348. doi:10.1016/S0022-0728(84)80328-9.

[44] V.A. Marichev, First experimental evaluation of partial charge transfer during anion adsorption, Colloids Surfaces A Physicochem. Eng. Asp. 348 (2009) 28–34. doi:10.1016/j.colsurfa.2009.06.027.

[45] E. Herrero, J.M. Feliu, Kinetics at Single Crystal Electrodes, in: Electrochem. Sci. a Sustain. Soc., Springer International Publishing, Cham, 2017: pp. 113–146. doi:10.1007/978-3-319-57310-6_5.

[46] K.A. Soliman, L.A. Kibler, Variation of the potential of zero charge for a silver monolayer deposited onto various noble metal single crystal surfaces, Electrochim. Acta. 52 (2007) 5654–5658. doi:10.1016/j.electacta.2006.12.070.

[47] D.D. Bode, T.N. Andersen, H. Eyring, Anion and pH effects on the potentials of zero charge of gold and silver electrodes, J. Phys. Chem. 71 (1967) 792–797. doi:10.1021/j100863a002.

[48] V.D. Jović, B.M. Jović, EIS and differential capacitance measurements onto single crystal faces in different solutions: Part I: Ag(111) in 0.01 M NaCl, J. Electroanal. Chem. 541 (2003) 1–11. doi:10.1016/S0022-0728(02)01309-8.

[49] B.M. Jović, V.D. Jović, D.M. Dražić, Kinetics of chloride ion adsorption and the mechanism of AgCl layer formation on the (111), (100) and (110) faces of silver, J. Electroanal. Chem. 399 (1995) 197–206. doi:10.1016/0022-0728(95)04291-1.

[50] B. Bozzini, L. D'Urzo, C. Mele, V. Romanello, A SERS Investigation of Cyanide Adsorption and Reactivity during the Electrodeposition of Gold, Silver, and Copper from Aqueous Cyanocomplexes Solutions, J. Phys. Chem. C. 112 (2008) 6352–6358. doi:10.1021/jp0726539.

[51] K.E. Brewer, C.M. Aikens, TDDFT investigation of surface-enhanced Raman scattering of HCN and CN(-) on Ag(20)., J. Phys. Chem. A. 114 (2010) 8858–63. doi:10.1021/jp1025174.

[52] D.D. Tuschel, J.E. Pemberton, J.E. Cook, SERS and SEM of roughened silver electrode surfaces formed by controlled oxidation-reduction in aqueous chloride media, Langmuir. 2 (1986) 380–388. doi:10.1021/la00070a002.

[53] A. Otto, A. Bruckbauer, Y.. Chen, On the chloride activation in SERS and single molecule SERS, J. Mol. Struct. 661–662 (2003) 501–514. doi:10.1016/j.molstruc.2003.07.026.

[54] C.M. Andersen, R. Bro, Practical aspects of PARAFAC modeling of fluorescence excitation-emission data, J. Chemom. 17 (2003) 200–215. doi:10.1002/cem.790.

[55] A. Wang, Y.-F. Huang, U.K. Sur, D.-Y. Wu, B. Ren, S. Rondinini, C. Amatore, Z.-Q. Tian, In Situ Identification of Intermediates of Benzyl Chloride Reduction at a Silver Electrode by SERS Coupled with DFT Calculations, J. Am. Chem. Soc. 132 (2010) 9534–9536. doi:10.1021/ja1024639.

[56] R. Pang, X.-G. Zhang, J.-Z. Zhou, D.-Y. Wu, Z.-Q. Tian, SERS Chemical Enhancement of Water Molecules from Halide Ion Coadsorption and Photoinduced Charge Transfer on Silver Electrodes, J. Phys. Chem. C. 121 (2017) 10445–10454. doi:10.1021/acs.jpcc.7b02408.

Figures caption

Fig. 1. Raman spectra for UA 0.2 mM in (a) $HClO_4$ 0.1 M and (b) $HClO_4$ 0.1 M + KCl $5 \cdot 10^{-3}$ M at different electrode potentials during the oxidation of the silver disk electrode. (c) LSV and (d) voltaRamangram at 641 cm^{-1} as a function of the potential applied for UA 0.2 mM in $HClO_4$ 0.1 M (blue curve) and UA 0.2 mM in $HClO_4$ 0.1 M + KCl $5 \cdot 10^{-3}$ M (red curve). Initial potential: +0.10 V. Final potential: +0.55 V. Scan rate: 0.02 $V \cdot s^{-1}$.

Fig. 2. ChronoRamangrams at 641 cm^{-1} (blue curves) and transient current (orange curves) for CA at (a) +0.40 V for 60 s and (b) +0.40 V for 30 s and measuring at OCP for 30 s. Solution: UA 0.2 mM + $HClO_4$ 0.1 M + KCl $5 \cdot 10^{-3}$ M.

Fig. 3. SEM images for the silver disk oxidation process in UA 0.2 mM + $HClO_4$ 0.1 M + KCl 5.10^{-3} M. Images taken at: (a) +0.36 V and (b) +0.49 V. Potentials referred to the Ag/AgCl electrode.

Fig. 4. VoltaRamangram (blue curves) for (a) Py $5 \cdot 10^{-2}$ M, (b) KCN $1 \cdot 10^{-2}$ M, (b) BzA $1 \cdot 10^{-2}$ M and (d) UA $2 \cdot 10^{-4}$ M in comparison with the corresponding CV (orange curves) on a silver disk electrode. Solution: probe molecule + HClO4 0.1 M + KCl $5 \cdot 10^{-3}$ M. Scan rate 0.02 $V \cdot s^{-1}$.

Fig. 5. Calibration curve for citric acid (orange points) using EC-SOERS. Treatment of the data performed using PARAFAC analysis. Solution: Citric acid X M + HClO4 0.1 M + KCl $5 \cdot 10^{-3}$ M. Scan rate 0.02 $V \cdot s^{-1}$.

Fig. 1

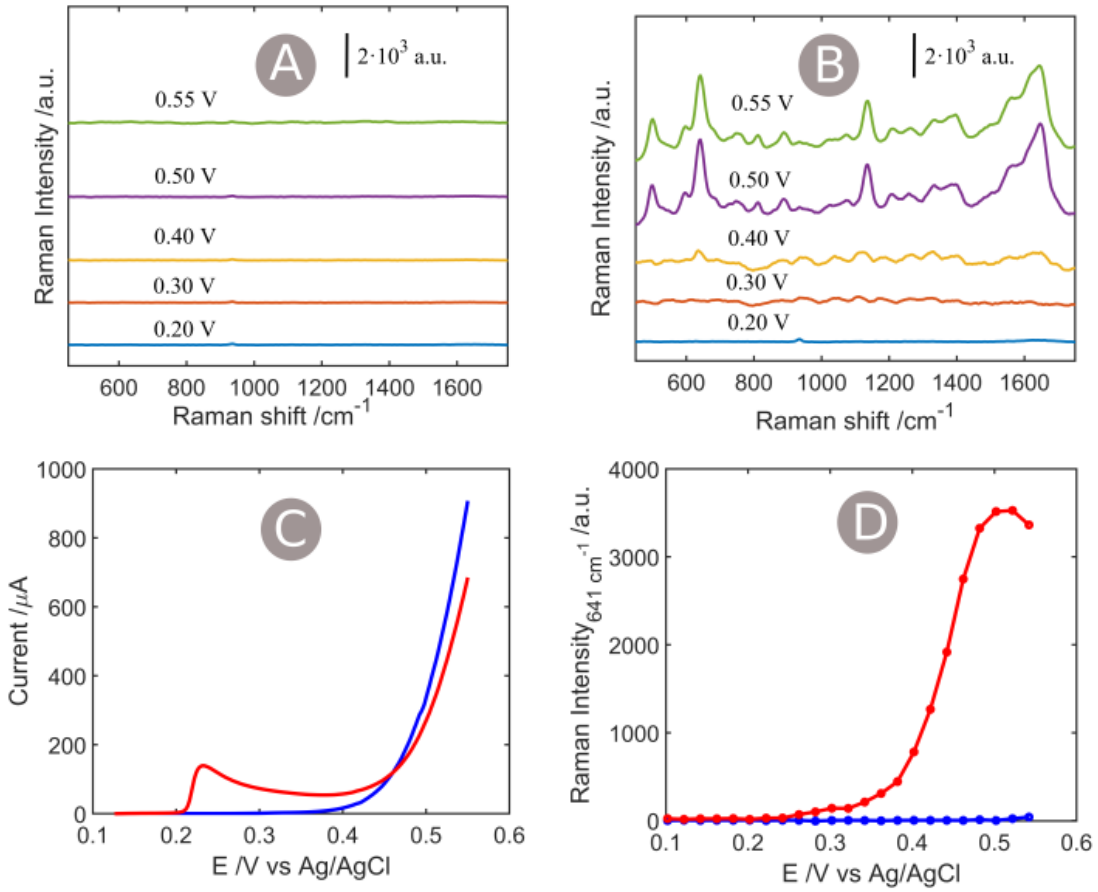
A
2·10^3 a.u.
0.55 V
0.50 V
0.40 V
0.30 V
0.20 V
Raman Intensity /a.u.
600 800 1000 1200 1400 1600
Raman shift /cm^-1
B
2·10^3 a.u.
0.55 V
0.50 V
0.40 V
0.30 V
0.20 V
Raman Intensity /a.u.
600 800 1000 1200 1400 1600
Raman shift /cm^-1
C
Current /μA
0 200 400 600 800 1000
0.1 0.2 0.3 0.4 0.5 0.6
E /V vs Ag/AgCl
D
Raman Intensity641 cm^-1 /a.u.
0 1000 2000 3000 4000
0.1 0.2 0.3 0.4 0.5 0.6
E /V vs Ag/AgCl

Fig. 2

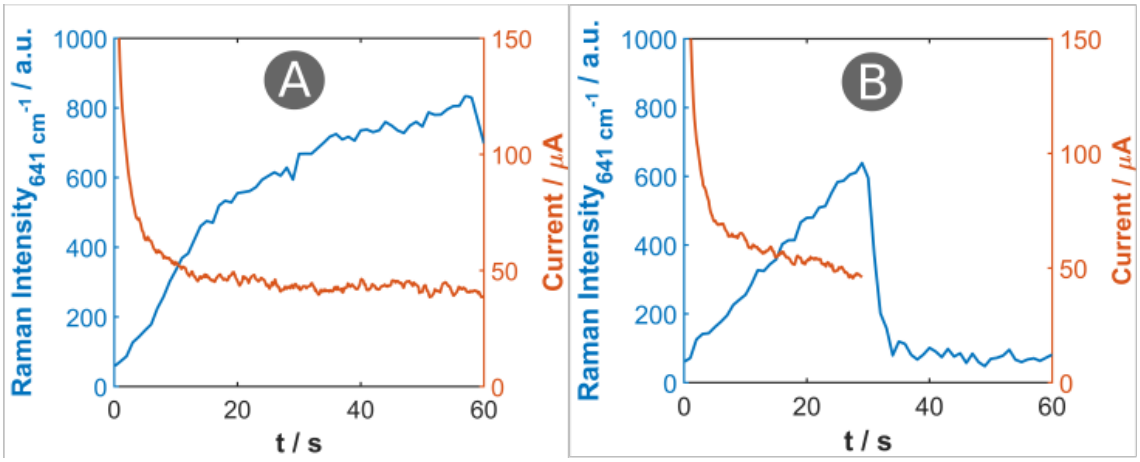
A
B
Raman Intensity641 cm-1 / a.u.
Current / μA
t / s
0
200
400
600
800
1000
0
50
100
150
0
20
40
60

Fig. 3

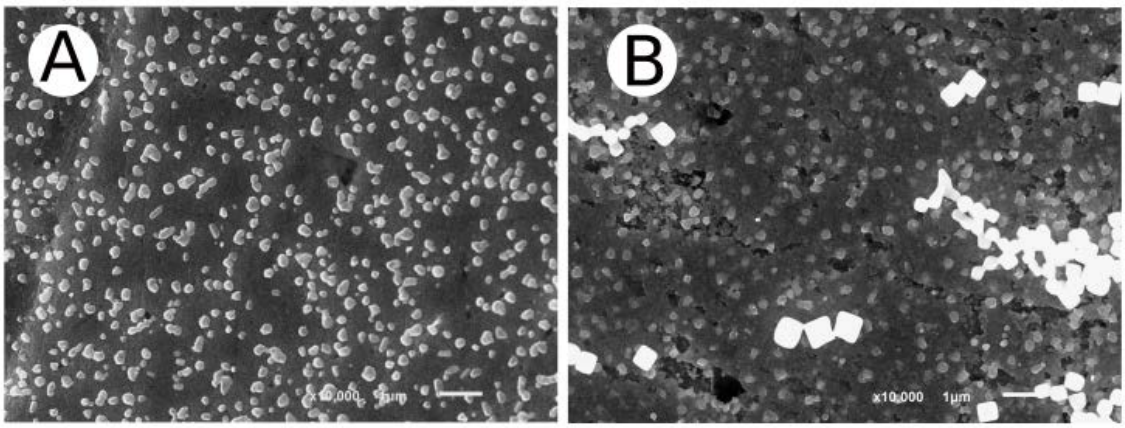

Fig. 4

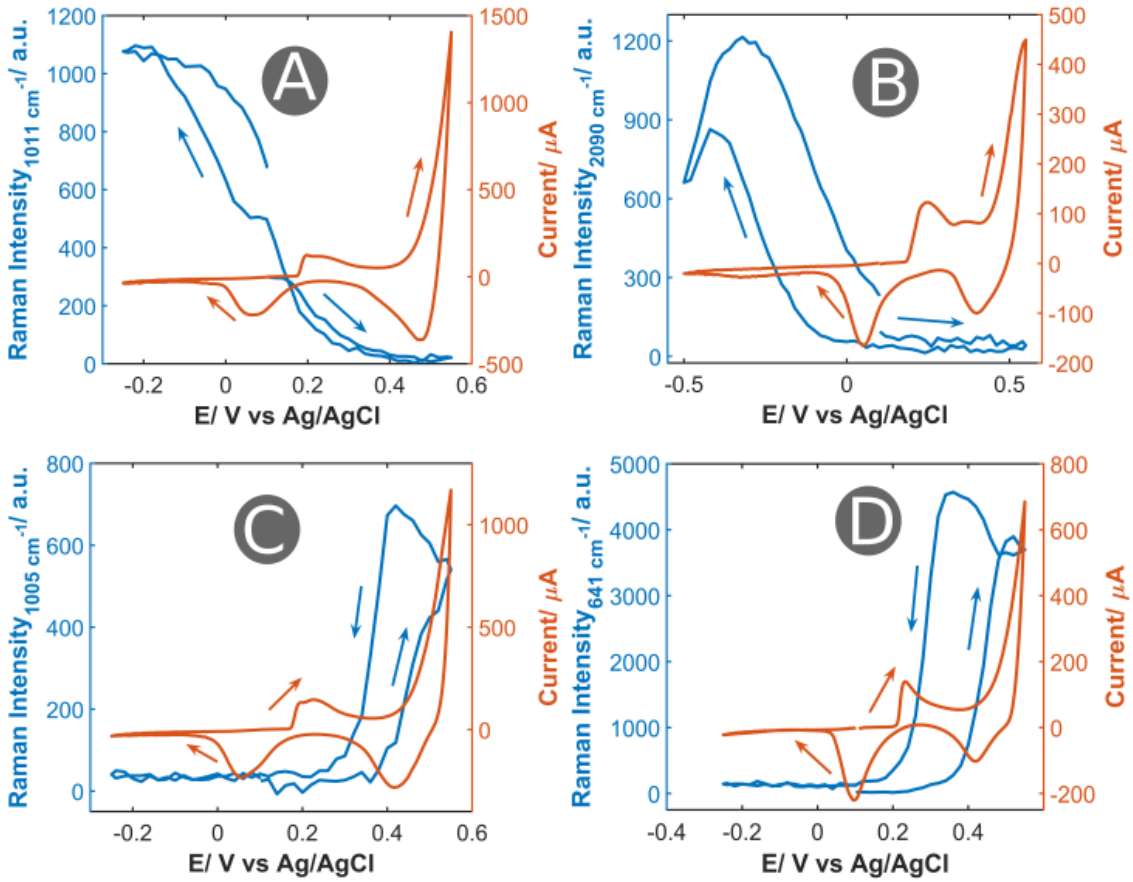
A
B
C
D
Raman Intensity 1011 cm-1/ a.u.
Raman Intensity 2090 cm-1/ a.u.
Raman Intensity 1005 cm-1/ a.u.
Raman Intensity 641 cm-1/ a.u.
Current/ μA
E/ V vs Ag/AgCl

Fig. 5

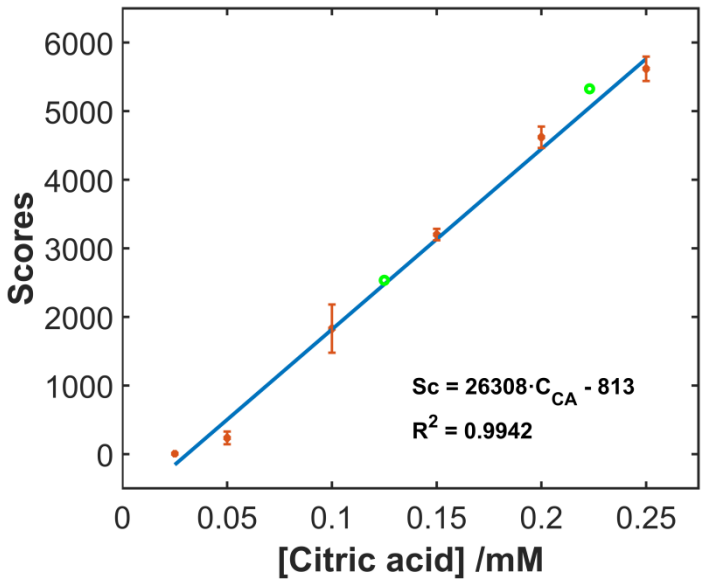
Scores
6000
5000
4000
3000
2000
1000
0
0
0.05
0.1
0.15
0.2
0.25
[Citric acid] /mM
Sc = 26308·C_CA - 813
R^2 = 0.9942